Experimental demonstration of fully contextual quantum correlations on an NMR quantum information processor

Dileep Singh,[*] Jaskaran Singh,[†] Kavita Dorai,[‡] and Arvind[§]
Department of Physical Sciences, Indian Institute of Science Education and Research Mohali, Mohali, Punjab 140306, India

(Received 27 March 2019; published 8 August 2019)

The existence of contextuality in quantum mechanics is a fundamental departure from the classical description of the world. Currently, the quest to identify scenarios which cannot be more contextual than quantum theory is at the forefront of research in quantum contextuality. In this work we experimentally test two inequalities, which are capable of revealing fully contextual quantum correlations, on a Hilbert space of dimension 8 and 4, respectively, on an NMR quantum information processor. The projectors associated with the contextuality inequalities are reformulated in terms of Pauli operators, which can be determined in an NMR experiment. We analyze the behavior of each inequality under rotation of the underlying quantum state, which unitarily transforms it to another pure state.

DOI: 10.1103/PhysRevA.100.022109

I. INTRODUCTION

Noncontextual hidden-variable (NCHV) theories in which outcomes of measurements do not depend on other compatible measurements have been shown not to reproduce quantum correlations [1,2]. Quantum mechanics (QM) exhibits the property of contextuality [3–5], which implies that measurement results of observables depend upon other commuting observables which are within the same measurement test. Much recent research has been in the direction of guessing the physical principle responsible for this form of contextuality [6]. The pertinent questions that arise include whether there is any theory more contextual than quantum mechanics and whether the simplest scenario in which more general theories cannot be more contextual than quantum mechanics can be identified [7–10].

Contextuality tests correspond to the violation of certain inequalities involving expectation values; the first such test was proposed by Kochen and Specker [2] by using a single-qutrit system [the Kochen-Specker (KS) theorem], and a modified KS scheme was constructed by Peres [11]. State-independent [12–14] tests use the set of observables such that for any quantum state there is no probability distribution which can describe the outcome of measurement of these observables on that state; hence these tests are able to reveal the contextual behavior of any state of the quantum system. On the other hand, the state-dependent [15–17] tests typically use fewer observables to show that no joint probability distribution can describe the measurement outcomes on a certain subset of states of the quantum system. The smallest indivisible physical system exhibiting quantum contextuality for repeatable measurements is a qutrit (a three-level quantum system) [1]. The simplest state-dependent noncontextual inequality, which is commonly referred to as the Klyachko-Can-Binicioglu-Shumovsky (KCBS) inequality [15], for a qutrit requires five experiments, each of them involving two compatible yes-no tests [7]. Several experimental tests of quantum contextuality have been demonstrated by different groups using photons [18–22], ions [23,24], neutrons [25], and nuclear spins [26,27].

In this paper we experimentally demonstrate fully contextual quantum correlations via two different inequalities, on an NMR quantum information processor. The first inequality, as proposed by Nagali *et al.* [21], uses ten projectors and ten measurements which we implement on states in a four-dimensional Hilbert space. The second inequality, proposed by Cabello [7], utilizes ten projectors and requires five measurements on a state in a Hilbert space of dimension at least 6. We demonstrate this inequality by realizing the six-dimensional subspace on states in an eight-dimensional Hilbert space. For experimental verification of both inequalities, we decompose all the projectors involved in terms of Pauli operators. The advantage is twofold: First, it reduces the need to perform quantum state tomography, which is a resource-intensive procedure, and second, the inequalities can be tested by using fewer observables. The eight-dimensional and four-dimensional Hilbert spaces are physically realized using three and two NMR qubits, respectively. Violation of the inequalities as observed experimentally match well with theoretical predictions and have an experimental fidelity greater than or equal to 0.96. We also study the behavior of both inequalities when the underlying quantum state undergoes a rotation. Our results imply that the violation of both inequalities follows a nonlinear trend with respect to the rotation angle of the underlying state. We also find that fully contextual quantum correlations on an eight-dimensional Hilbert space are more robust against state rotation as compared to those on the four-dimensional Hilbert space, allowing a greater angle for violation.

[*]dileepsingh@iisermohali.ac.in
[†]jaskaransinghnirankari@iisermohali.ac.in
[‡]kavita@iisermohali.ac.in
[§]arvind@iisermohali.ac.in

The material in this paper is arranged as follows. Section II describes fully contextual quantum correlations in a four-dimensional Hilbert space and its experimental implementation using two NMR qubits. Section III describes a similar scenario, albeit on an eight-dimensional quantum system experimentally realized using three NMR qubits. Section IV contains a summary and a few concluding remarks. Details of the decomposition of the projectors in terms of Pauli operators for the four-dimensional and the eight-dimensional Hilbert space are given in Appendixes A and B, respectively.

II. FULLY CONTEXTUAL QUANTUM CORRELATIONS IN A FOUR-DIMENSIONAL HILBERT SPACE

In this section we first review a contextuality inequality which is capable of revealing fully contextual quantum correlations as developed by Nagali *et al.* [21] which utilize states in a Hilbert space of dimension at least 4. We provide a modified version of the inequality by decomposition into Pauli matrices which we experimentally test on a four-level quantum system using two NMR qubits.

The simplest test of quantum contextuality requires the measurement of five different projectors $\{\Pi_i\}$, $i \in \{0, 1, 2, 3, 4\}$, and $\Pi_i = |v_i\rangle\langle v_i|$, where $|v_i\rangle$ are unit vectors [15]. These projectors follow the exclusivity relation $P(\Pi_i = 1) + P(\Pi_{i\oplus 1} = 1) = 1$, where $P(\Pi_i = 1)$ represents the probability of obtaining the outcome Π_i and addition is taken modulo 5. For projective measurements, this relationship implies that only one of Π_i or $\Pi_{i\oplus 1}$ can be obtained in a joint measurement of both. The corresponding test, termed KCBS inequality [7], is of the form

$$\frac{1}{2}\sum_{i=0}^{4} P(\Pi_i + \Pi_{i\oplus 1} = 1) \overset{\text{NCHV}}{\leqslant} 2 \overset{\text{QM}}{\leqslant} \sqrt{5} \overset{\text{GP}}{\leqslant} \frac{5}{2}, \tag{1}$$

where the inequalities correspond to the maximum value achievable for NCHV theories, QM, and generalized probabilistic (GP) theories.

As is evident from Eq. (1), the maximum violation that can be achieved in quantum mechanics is less than what can be attained if an underlying GP model is considered. Therefore, for the KCBS scenario, quantum correlations are not fully contextual. Recently, it has been shown that there exist tests of contextuality for which quantum correlations saturate the bound as imposed by GP models [28]. For these scenarios, quantum correlations are either noncontextual or fully contextual.

Fully contextual quantum correlations can also be achieved for various other scenarios, one of which is shown in Ref. [21] and entails measurements corresponding to ten different projectors $\Pi_j = |u_j\rangle\langle u_j|$, $j = \{0, 1, \ldots, 9\}$. In this particular scenario, the projectors follow exclusivity relationships as depicted in Fig. 1, where each vertex represents a projector Π_i and two projectors are connected by an edge if and only if they are exclusive. The corresponding test of contextuality is then given by the inequality

$$\mathcal{C} = \sum_{i=0}^{9} P(\Pi_i = 1) \overset{\text{NCHV}}{\leqslant} 3 \overset{\text{QM,GP}}{\leqslant} \frac{7}{2}. \tag{2}$$

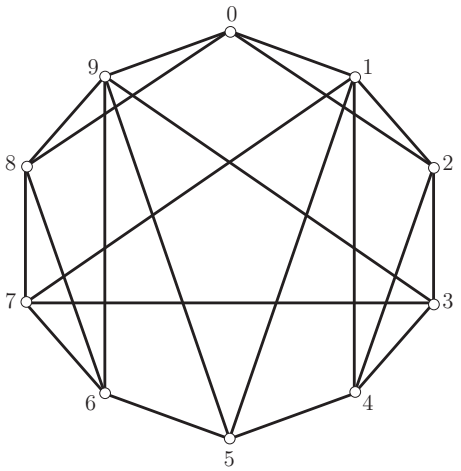

FIG. 1. Orthogonality graph corresponding to the inequality $\mathcal{C}$. Vertices correspond to projectors and two vertices are connected by an edge if they are orthogonal.

This test requires ten different measurements rather than five and is capable of revealing fully contextual quantum correlations in a Hilbert space of minimum dimension 4. The inequality can be explicitly tested if we consider the unit vectors $|u_i\rangle$ as follows:

$$\langle u_0| \equiv \frac{1}{\sqrt{2}}(0, 0, 1, 1), \tag{3a}$$

$$\langle u_1| \equiv \frac{1}{2}(1, -1, 1, -1), \tag{3b}$$

$$\langle u_2| \equiv \frac{1}{2}(1, -1, -1, 1), \tag{3c}$$

$$\langle u_3| \equiv \frac{1}{\sqrt{2}}(1, 0, 0, -1), \tag{3d}$$

$$\langle u_4| \equiv \frac{1}{2}(1, 1, 1, 1), \tag{3e}$$

$$\langle u_5| \equiv \frac{1}{\sqrt{2}}(0, 1, 0, -1), \tag{3f}$$

$$\langle u_6| \equiv \frac{1}{2}(-1, 1, 1, 1), \tag{3g}$$

$$\langle u_7| \equiv \frac{1}{\sqrt{2}}(1, 0, 0, 1), \tag{3h}$$

$$\langle u_8| \equiv \frac{1}{2}(1, 1, 1, -1), \tag{3i}$$

$$\langle u_9| \equiv \frac{1}{2}(1, 1, -1, 1). \tag{3j}$$

The corresponding projective measurements are of the form

$$\mathcal{M}_j = \{\Pi_j, I - \Pi_j\} \forall\, j \in \{0, 1, \ldots, 9\}, \tag{4}$$

which are performed on the state

$$\langle\phi| \equiv (0, 0, 0, 1). \tag{5}$$

To experimentally test the inequality $\mathcal{C}$ on a four-level quantum system using two NMR qubits, one has to

determine the expectation value of the observables involved for an experimentally prepared state. This can be achieved by decomposing the observables as a linear superposition of Pauli operators. For a two-qubit system any observable can be decomposed as a linear superposition of 16 Pauli operators, and the Pauli operator can be mapped to the single-qubit Pauli Z operator. This mapping is particularly useful in the context of an NMR experimental setup where the expectation value of the Z operator is easily accessible. In an NMR measurement schema, the observed z magnetization of a nuclear spin in a particular quantum state is proportional to the expectation value of the Z operator of the spin in that state. The time-domain NMR signal, i.e., the free-induction decay with an appropriate phase, results in Lorentzian peaks when Fourier transformed. These normalized experimental intensities give an estimate of the expectation value of Z in that quantum state [27,29,30].

For the experimental implementation of the inequality, we decompose the projectors $\{\Pi_j\}$ in terms of Pauli operators $\{I, X, Y, Z\}$ (details given in Appendix A). The inequality (2) can be rewritten in terms of expectation values as

$$\mathcal{C} = \sum_{i=0}^{9} \langle \Pi_i \rangle = \sum_{i=0}^{9} \mathrm{Tr}[\Pi_i \rho'], \tag{6}$$

where $\rho' = |\phi\rangle\langle\phi|$. Using Eqs. (2), (6), and (A1), the inequality $\mathcal{C}$ can be rewritten as

$$\mathcal{C} = \tfrac{1}{4}\mathrm{Tr}[B\rho'] \overset{\text{NCHV}}{\leqslant} 3 \overset{\text{QM,GP}}{\leqslant} \tfrac{7}{2}, \tag{7}$$

where

$$B = XX + YY - ZI + 2ZZ - IZ + 10II, \tag{8}$$

which can be experimentally verified as detailed below.

The underlying state $|\phi\rangle$ is unitarily rotated by an angle θ as

$$|\phi(\theta)\rangle = U_\theta I |\phi\rangle, \tag{9}$$

where

$$U_\theta = \begin{bmatrix} \cos\frac{\theta}{2} & -\sin\frac{\theta}{2} \\ \sin\frac{\theta}{2} & \cos\frac{\theta}{2} \end{bmatrix}. \tag{10}$$

The corresponding theoretical value of the inequality $\mathcal{C}$ for the aforementioned state (9) is found to be $\mathcal{C} = \frac{1}{4}(11 + 3\cos\theta)$ and is plotted in Fig. 5 along with the experimentally observed values at various θ angles.

For instance, in order to determine the expectation value $\langle XX \rangle$ for the state $\rho = |\psi\rangle\langle\psi|$, we map the state ρ to $\rho_1 = U_1 \rho U_1^\dagger$, where $U_1 = \mathrm{CNOT}_{12} Y_2 Y_1$, followed by observing $\langle Z_2 \rangle$ for the state ρ_1. The expectation value $\langle Z_2 \rangle$ for the state ρ_1 is equivalent to observing the expectation value of $\langle XX \rangle$ for the state ρ [30]. Table I details the mapping of Pauli basis operators (used in this paper) to the single-qubit Z operator. The observables of interest are given in the decomposition of Eq. (8). By experimentally evaluating the expectation value of the observables given in Eq. (8), the value of $\mathcal{C}$ can be estimated.

To implement the inequality on a four-dimensional quantum system, the molecule of ^{13}C-enriched chloroform dissolved in acetone-D6 was used, with the ^{1}H and ^{13}C spins being labeled as qubit 1 and qubit 2, respectively (see Fig. 2 and Table II for details of the experimental parameters).

TABLE I. Product operators for a two-qubit system mapped onto the Pauli Z operators by transforming the initial state $\rho \to \rho_i = U_i \rho U_i^\dagger$.

Observable	Unitary operator
$\langle XX \rangle = \mathrm{Tr}[\rho_1 Z_2]$	$U_1 = \mathrm{CNOT}_{12}\, Y_2 Y_1$
$\langle YY \rangle = \mathrm{Tr}[\rho_2 Z_2]$	$U_2 = \mathrm{CNOT}_{12}\, X_2 X_1$
$\langle ZI \rangle = \mathrm{Tr}[\rho_3 Z_1]$	$U_3 =$ identity
$\langle ZZ \rangle = \mathrm{Tr}[\rho_4 Z_2]$	$U_4 = \mathrm{CNOT}_{12}$
$\langle IZ \rangle = \mathrm{Tr}[\rho_5 Z_2]$	$U_5 =$ identity

The Hamiltonian for a two-qubit system is given by [30]

$$\mathcal{H} = -\nu_H I_z^H - \nu_C I_z^C + J_{HC} I_z^H I_z^C, \tag{11}$$

where ν_H and ν_C are the chemical shifts, I_z^H and I_z^C are the z components of the spin angular momentum operators of the ^{1}H and ^{13}C spins, respectively, and J_{HC} is the scalar coupling constant. The system was initialized in the pseudopure state (PPS) $|00\rangle$, using a spatial averaging technique [31,32] with the density operator given by

$$\rho_{00} = \tfrac{1}{4}(1-\epsilon) I_4 + \epsilon |00\rangle\langle 00|, \tag{12}$$

where I_4 is the 4×4 identity operator and ϵ is proportional to the spin polarization and can be evaluated from the ratio of magnetic and thermal energies of an ensemble of magnetic moments μ in a magnetic field B at temperature T; $\epsilon \sim \frac{\mu B}{k_B T}$ and at room temperature and for $B \approx 10$ T, $\epsilon \approx 10^{-5}$. The state fidelity of the experimentally prepared PPS was computed to be 0.99. For the experimental reconstruction of the density operator full quantum state tomography was performed using a set of preparatory pulses $\{II, IX', IY', X'X'\}$, where I implies no operation and $X'(Y')$ denotes a qubit-

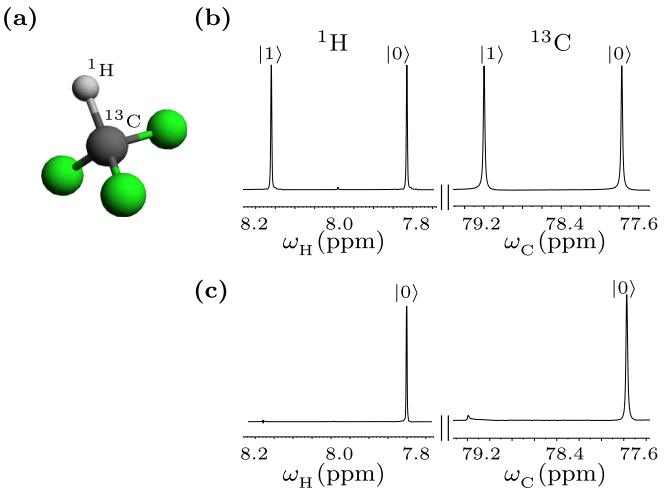

FIG. 2. (a) Molecular structure of ^{13}C-labeled chloroform used as a two-qubit quantum system. Also shown are the NMR spectra of (b) the thermal equilibrium state and (c) the pseudopure state $|00\rangle$. Each peak is labeled with the logical state of the qubit which is passive during the transition. The horizontal scale represents the chemical shifts in ppm.

TABLE II. NMR parameters for ^{13}C-labeled chloroform used as a two-qubit quantum system.

Qubit	ν (Hz)	J (Hz)	T_1 (s)	T_2 (s)
^{1}H	4787.86	$J_{HC} = 215.11$	7.9	2.95
^{13}C	11814.09		16.6	0.3

selective radio-frequency (rf) pulse of flip angle 90° of phase $x(y)$. The durations of $\frac{\pi}{2}$ pulses for ^{1}H and ^{13}C nuclei were 9.56 μs at a power level of 18.14 W and 16.15 μs at a power level of 179.47 W, respectively.

The quantum circuit to achieve the required states to test the inequality $\mathcal{C}$ on a four-dimensional quantum system is shown in Fig. 3(a) and the corresponding NMR pulse sequence is shown in Fig. 3(b). Eight different states were generated by varying the flip angle θ over a range of values: 180°, 120°, 90°, 69.23°, 60°, 45°, 30°, and 0°. The state that is prepared with the flip angle $\theta = 180°$ gives the minimum value of $\mathcal{C}$, while the state which is prepared without applying any rf pulse ($\theta = 0°$) gives the maximum value. All the states required for testing the inequality on the four-dimensional quantum system were experimentally prepared with state fidelities greater than or equal to 0.97. The tomograph for one such experimentally prepared state with the flip angle $\theta = 180°$ and state fidelity 0.99 is depicted in Fig. 4.

For each of these eight different initial states, the contextuality test was repeated three times. The mean values and the corresponding error bars were calculated and the results are shown in Fig. 5, where the inequality values are plotted for different θ values. The maximum of the sum of probabilities using classical theory is 3 and the maximum of the sum of probabilities using quantum theory is 3.5, which are shown by dotted and dashed lines, respectively, in Fig 5. As can be seen from the values tabulated in Table III, the theoretically computed and experimentally measured values of the inequality agree well to within experimental errors. From Fig. 5 it can be seen that the violation for the inequality $\mathcal{C}$ decreases as the original state $|\phi\rangle$ is rotated through an angle θ; no violation is observed for the angle $\theta > 70°$. The corresponding curve is found to obey a nonlinear trend such that smaller rotations lead to minor changes in the violation, while larger rotations may lead to a situation where no violation is observed.

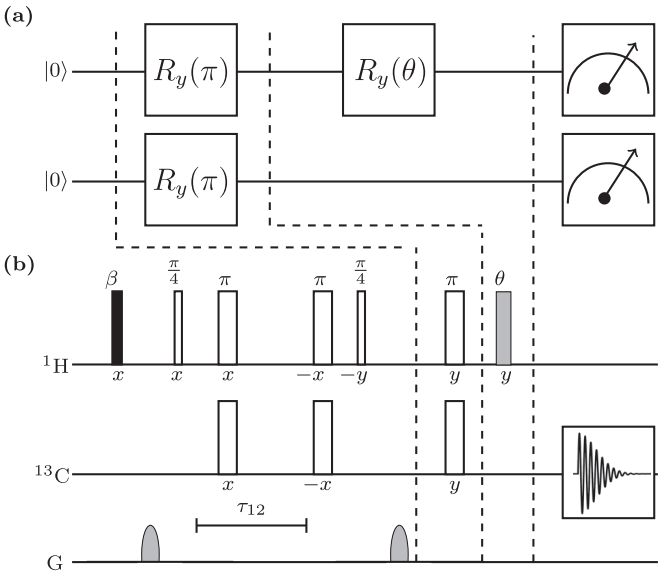

FIG. 3. (a) Quantum circuit for the required state, generated randomly with the different flip angles. (b) NMR pulse sequence for the corresponding quantum circuit. The sequence of pulses before the first dashed black line achieves state initialization into the $|00\rangle$ state. The value of the flip angle β is kept fixed at 59.69°, while the pulse rf flip angle θ is varied. The time interval τ_{12} is set to $\frac{1}{2J_{HC}}$.

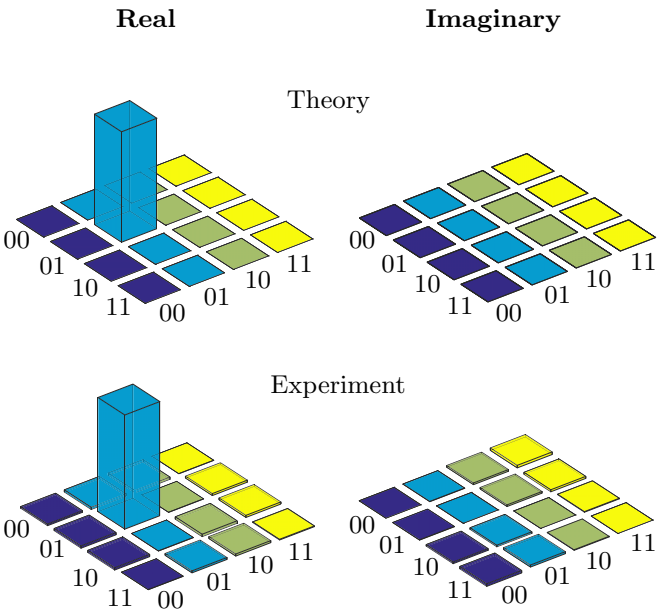

FIG. 4. Real (left) and imaginary (right) parts of the theoretical and experimental tomographs of the $\langle\phi_1| = (0, -1, 0, 0)$ state in the four-dimensional Hilbert space, prepared with an experimental state fidelity of 0.99.

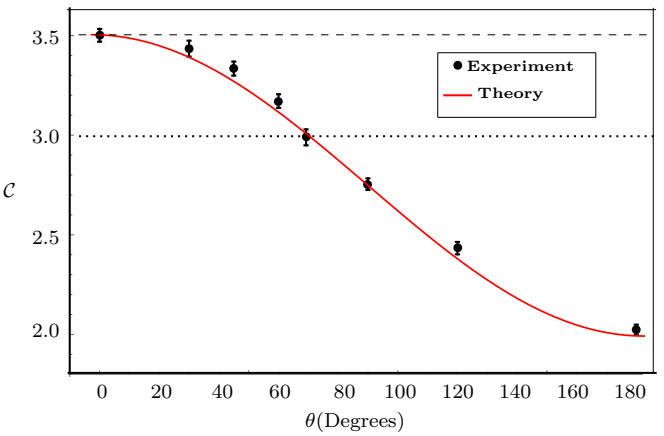

FIG. 5. Quantum correlations corresponding to the inequality $\mathcal{C}$ for various states plotted for different initial states $|\phi\rangle$ as a function of the θ parameter.

TABLE III. Theoretically computed and experimentally measured values of quantum correlations corresponding to the inequality $\mathcal{C}$ for different quantum states parametrized by the angle θ.

θ	Theory	Expt.
180°	2.000	2.024 ± 0.025
120°	2.375	2.433 ± 0.031
90°	2.750	2.754 ± 0.029
69.23°	3.016	2.989 ± 0.040
60°	3.125	3.171 ± 0.034
45°	3.280	3.334 ± 0.035
30°	3.399	3.434 ± 0.040
0°	3.500	3.501 ± 0.032

III. FULLY CONTEXTUAL QUANTUM CORRELATIONS IN AN EIGHT-DIMENSIONAL HILBERT SPACE

In this section we first review a contextuality inequality which is capable of revealing fully contextual quantum correlations as developed by Cabello [7], which requires a Hilbert space dimensionality of at least 6. We then design a modified version of the inequality via decomposition of the projectors into Pauli matrices, for ease of experimental implementation. We experimentally test the inequality on an eight-level quantum system, physically realized via three NMR qubits.

One of the simplest tests of contextuality, capable of revealing fully contextual quantum correlations, requires only five measurements, but of ten different projectors $\{\Pi_i\}$, and is of the form

$$\mathcal{K} = \frac{1}{2}\sum_{i=0}^{4} P(\Pi_i + \Pi_{i+1} + \Pi_{i+5} + \Pi_{i+7} = 1) \overset{\text{NCHV}}{\leqslant} 2 \overset{\text{QM,GP}}{\leqslant} \frac{5}{2}, \tag{13}$$

where the sum in the indices is defined as standard addition except for three cases where we define it as $4+1=0$, $3+7=5$, and $4+7=6$ to ensure that only those vertices connected by the same edge style in Fig. 6 appear in the sum. To elaborate, the term corresponding to $i=4$ will be of the form $P(\Pi_4 + \Pi_0 + \Pi_9 + \Pi_6 = 1)$.

Since both the KCBS and the aforementioned inequality (13) require only five different measurements, the above scenario is termed a KCBS twin inequality, with the only difference that it is capable of revealing fully contextual quantum correlations and requires quantum systems having Hilbert space dimension at least 6. We will henceforth refer to this inequality as the KCBS twin inequality.

The scenario corresponding to the KCBS twin inequality (13) can be represented by an exclusivity graph as shown in Fig. 6. In this graph, each vertex corresponds to a unit vector $|v_i\rangle$ used to construct the projectors Π_i, and two vertices are connected by an edge if and only if they are exclusive. From the graph it is possible to identify five different measurements $\mathcal{M}_i$, which are defined as

$$\mathcal{M}_i = \{\Pi_i, \Pi_{i+1}, \Pi_{i+5}, \Pi_{i+7}\}\, \forall\, i \in \{0, 1, \ldots, 9\}. \tag{14}$$

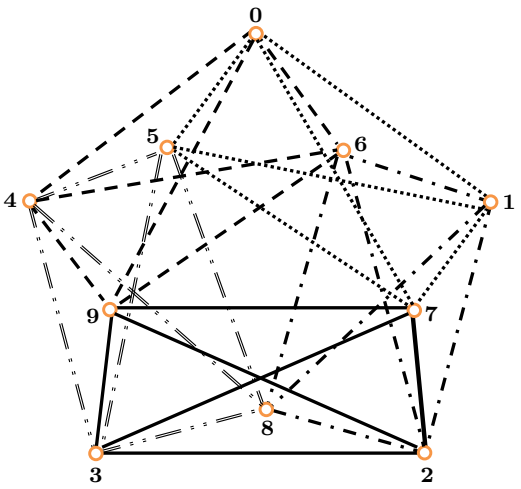

FIG. 6. Orthogonality graph corresponding to the KCBS twin inequality $\mathcal{K}$. Vertices correspond to projectors, while edges represent the orthogonality relationship between two vertices. Five sets of four interconnected vertices correspond to measurements involved in testing $\mathcal{K}$ and are differentiated by different edge line styles.

These measurements can be identified from the graph in Fig. 6 by five sets of four interconnected vertices, each represented by a different line style.

An explicit form of the KCBS twin inequality (13) which saturates the QM and GP bound can be obtained if we consider the unit vectors $|v_i\rangle$ defined as

$$\langle v_0| \equiv \frac{1}{\sqrt{8}}(\sqrt{2}, -\sqrt{2}, 0, 0, 2, 0, 0, 0), \tag{15a}$$

$$\langle v_1| \equiv \frac{1}{\sqrt{8}}(\sqrt{2}, 0, 0, \sqrt{2}, -1, \sqrt{3}, 0, 0), \tag{15b}$$

$$\langle v_2| \equiv \frac{1}{2}(1, -1, -1, -1, 0, 0, 0, 0), \tag{15c}$$

$$\langle v_3| \equiv \frac{1}{2}(1, -1, 1, 1, 0, 0, 0, 0), \tag{15d}$$

$$\langle v_4| \equiv \frac{1}{\sqrt{8}}(\sqrt{2}, 0, 0, -\sqrt{2}, -1, \sqrt{3}, 0, 0), \tag{15e}$$

$$\langle v_5| \equiv \frac{1}{\sqrt{8}}(\sqrt{2}, 0, -\sqrt{2}, 0, -1, -\sqrt{3}, 0, 0), \tag{15f}$$

$$\langle v_6| \equiv \frac{1}{\sqrt{8}}(\sqrt{2}, 0, \sqrt{2}, 0, -1, -\sqrt{3}, 0, 0), \tag{15g}$$

$$\langle v_7| \equiv \frac{1}{2}(1, 1, 1, -1, 0, 0, 0, 0), \tag{15h}$$

$$\langle v_8| \equiv \frac{1}{\sqrt{8}}(\sqrt{2}, \sqrt{2}, 0, 0, 2, 0, 0, 0), \tag{15i}$$

$$\langle v_9| \equiv \frac{1}{2}(1, 1, -1, 1, 0, 0, 0, 0). \tag{15j}$$

The state $|\psi\rangle$ on which the measurements $\mathcal{M}_i$ will be performed is chosen as

$$\langle\psi| \equiv (1, 0, 0, 0, 0, 0, 0, 0) \tag{16}$$

so that $\langle v_i|\psi\rangle = \frac{1}{2}\,\forall\, i \in \{0, 1, \ldots, 9\}$, which subsequently ensures the exclusivity relation $P(\Pi_i + \Pi_{i+1} + \Pi_{i+5} + \Pi_{i+7} = 1) = 1, i = 0, 1, \ldots, 4$.

To experimentally test the inequality $\mathcal{K}$ [Eq. (13)] on a eight-level quantum system using three NMR qubits, the expectation values of the observables involved have to be determined for an experimentally prepared state. The expectation value of desired observables can be determined by decomposing the observables as a linear superposition of the Pauli operators as has been detailed in Sec. II. For a three-qubit system any observable can be decomposed as a linear superposition of 64 Pauli basis operators.

In order to evaluate the KCBS twin inequality experimentally, we first decompose the projectors involved in terms of Pauli operators $\{I, X, Y, Z\}$ for three qubits (details given in Appendix B). Since in an NMR quantum information processor it is only possible to measure the expectation value of the observables, we first translate Eq. (13) in terms of expectation values as

$$\mathcal{K} = \frac{1}{2}\sum_{i=0}^{4}\langle \Pi_i + \Pi_{i+1} + \Pi_{i+5} + \Pi_{i+7}\rangle$$
$$= \sum_{i=0}^{9}\langle \Pi_i\rangle = \sum_{i=0}^{9}\mathrm{Tr}[\Pi_i\rho], \tag{17}$$

where $\rho = |\psi\rangle\langle\psi|$.

Using the decomposition given in Eq. (B1), the inequality $\mathcal{K}$ [Eq. (13)] can then be rewritten as

$$\mathcal{K} = \tfrac{1}{8}\mathrm{Tr}[A\rho] \overset{\text{NCHV}}{\leqslant} 2 \overset{\text{QM,GP}}{\leqslant} \tfrac{5}{2} \tag{18}$$

and

$$A = IIZ + 4IZI + IZZ + 4ZII \tag{19}$$
$$+ ZIZ - 2ZZI + ZZZ + 10III. \tag{20}$$

which we experimentally verify using a three-qubit NMR information processor. We note here in passing that the decomposition of the observable A consists only of diagonal Pauli operators, which can be easily observed in an experiment. The fact that the observable A can be decomposed as a combination of only diagonal Pauli operators is an interesting coincidence. Furthermore, in an NMR setup, it is easier to implement these diagonal operators as compared to other operators which have diagonal and off-diagonal terms. For example, the expectation value of $\langle IIZ\rangle$ can be obtained simply by measuring the NMR peak intensities after applying a detection pulse on the third qubit. The underlying state $|\psi\rangle$ is unitarily rotated by an angle θ as

$$|\psi(\theta)\rangle = U_\theta II|\psi\rangle, \tag{21}$$

where U_θ is as given in Eq. (10).

For the aforementioned state (21), the theoretical value of the inequality (18) is found to be $\mathcal{K} = \frac{1}{2}(4 + \cos\theta)$, which is plotted in Fig. 10 along with the experimentally observed values at various θ angles. By experimentally measuring the expectation value of the observable A for state ρ, the value of inequality $\mathcal{K}$ can be estimated. For example, in order to determine $\langle IZZ\rangle$, the underlying state ρ is mapped to the state $\rho_3 = U_3\rho U_3^\dagger$ with $U_3 = \mathrm{CNOT}_{23}$, followed by measuring $\langle Z_3\rangle$, which is equivalent to the expectation value of $\langle IZZ\rangle$ for the state ρ. The explicit mapping of the expectation value of the observables onto Pauli Z operators for three qubits is given in Table IV.

TABLE IV. Product operators for a three-qubit system mapped to the Pauli Z operators by transforming the initial state $\rho \to \rho_i = U_i\rho U_i^\dagger$.

Observable	Unitary operator
$\langle IIZ\rangle = \mathrm{Tr}[\rho_1 Z_3]$	$U_1 =$ identity
$\langle IZI\rangle = \mathrm{Tr}[\rho_2 Z_2]$	$U_2 =$ identity
$\langle IZZ\rangle = \mathrm{Tr}[\rho_3 Z_3]$	$U_3 = \mathrm{CNOT}_{23}$
$\langle ZII\rangle = \mathrm{Tr}[\rho_4 Z_1]$	$U_4 =$ identity
$\langle ZIZ\rangle = \mathrm{Tr}[\rho_5 Z_3]$	$U_5 = \mathrm{CNOT}_{13}$
$\langle ZZI\rangle = \mathrm{Tr}[\rho_6 Z_2]$	$U_6 = \mathrm{CNOT}_{12}$
$\langle ZZZ\rangle = \mathrm{Tr}[\rho_7 Z_3]$	$U_7 = \mathrm{CNOT}_{23}\mathrm{CNOT}_{12}$

To experimentally implement the KCBS twin inequality capable of revealing fully contextual quantum correlations for an eight-dimensional quantum system, we used the molecule of ^{13}C -labeled diethyl fluoromalonate dissolved in acetone-D6, with the ^{1}H, ^{19}F, and ^{13}C spin-$\frac{1}{2}$ nuclei being encoded as qubit 1, qubit 2, and qubit 3, respectively (see Fig. 7 for the molecular structure and corresponding NMR spectrum of the PPS state, and Table V for details of the experimental NMR parameters). The NMR Hamiltonian for a three-qubit system

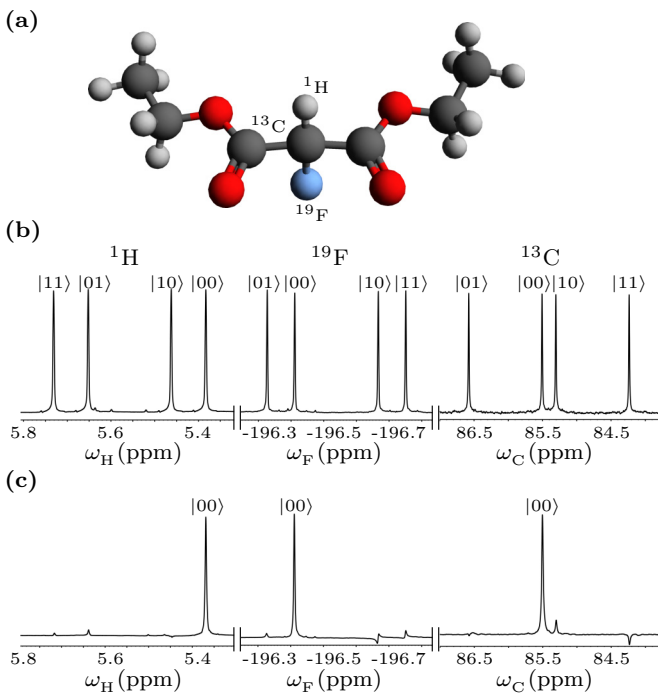

FIG. 7. (a) Molecular structure of ^{13}C-labeled diethyl fluoromalonate used to physically realize three qubits. Also shown are the NMR spectra of (b) the thermal equilibrium state and (c) the pseudopure state $|000\rangle$. Each peak is labeled with the logical state of the qubit which is passive during the transition. The horizontal scale represents the chemical shifts in ppm.

TABLE V. NMR parameters for the three-qubit ^{13}C-labeled diethyl fluoromalonate system.

Qubit	ν (Hz)	J (Hz)	T_1 (s)	T_2 (s)
^{1}H	3334.24	$J_{HF} = 47.5$	3.4	1.6
^{19}F	−110999.94	$J_{HC} = 161.6$	3.7	1.5
^{13}C	12889.53	$J_{FC} = -191.5$	3.6	1.3

is given by [29]

$$\mathcal{H} = -\sum_{i=1}^{3} \nu_i I_z^i + \sum_{i>j,i=1}^{3} J_{ij} I_z^i I_z^j, \tag{22}$$

where the indices $i, j = 1, 2$, or 3 label the qubit, ν_i is the chemical shift of the ith qubit in the rotating frame, J_{ij} is the scalar coupling interaction strength, and I_z^i is the z component of the spin angular momentum operator of the ith qubit. The system was initialized in a PPS, i.e., $|000\rangle$, using the spatial averaging technique [33] with the density operator given by

$$\rho_{000} = \frac{1-\epsilon}{2^3} I_8 + \epsilon |000\rangle\langle 000|, \tag{23}$$

where ϵ is proportional to the spin polarization and I_8 is the 8×8 identity operator. The fidelity of the experimentally prepared PPS state was computed to be 0.96 using the fidelity measure [34]. Full quantum state tomography [35,36] was performed to experimentally reconstruct the density operator via a set of preparatory pulses $\{III, IIY', IY'Y', Y'II, X'Y'X', X'X'Y', X'X'X'\}$, where I implies no operation and $X'(Y')$ denotes a qubit-selective rf pulse of flip angle 90° of phase $x(y)$.

Experiments were performed at room temperature (294 K) on a Bruker Avance III 600-MHz FT-NMR spectrometer equipped with a QXI probe. Local unitary operations were achieved by using highly accurate and calibrated spin-selective transverse rf pulses of suitable amplitude, phase, and duration. Nonlocal unitary operations were achieved by free evolution under the system Hamiltonian, of suitable duration under the desired scalar coupling with the help of embedded

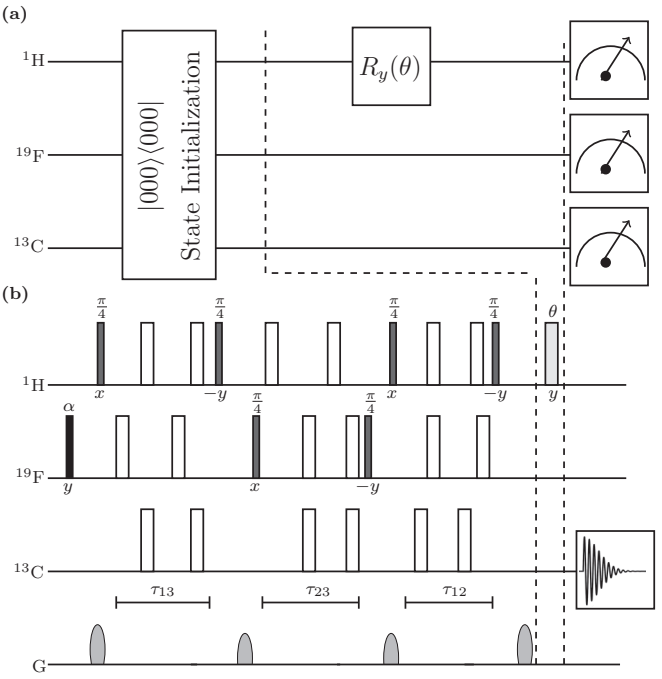

FIG. 8. (a) Quantum circuit for state preparation. The parameter θ in the unitary $R_y(\theta)$ is used to generate different quantum states. (b) Corresponding NMR pulse sequence for the quantum circuit. The sequence of pulses before the first dashed black line achieves initialization of the state into the pseudopure $|000\rangle$ state. The value of the flip angle α is kept fixed at 57.87°, while the flip angle θ is varied over a range of values. The broad open rectangles denote π pulses, and the flip angle and phases of the other pulses are written below each pulse. The time intervals τ_{12}, τ_{13}, and τ_{23} are set equal to $\frac{1}{2J_{HF}}$, $\frac{1}{2J_{HC}}$, and $\frac{1}{2J_{FC}}$, respectively.

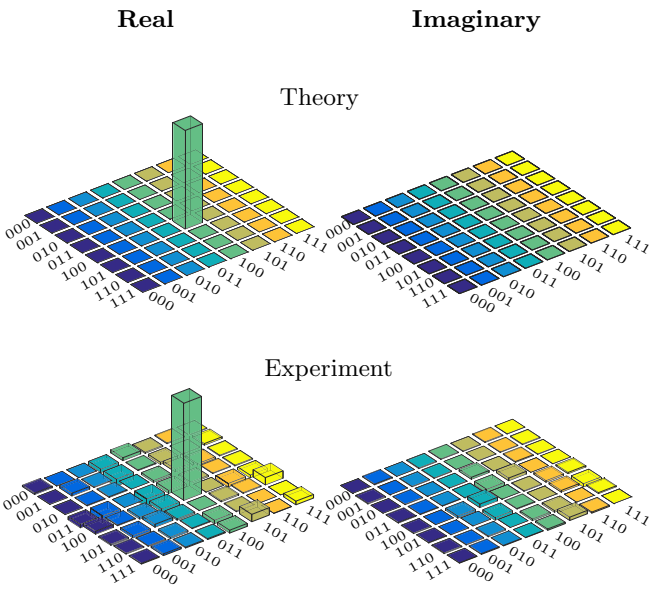

FIG. 9. Real (left) and imaginary (right) parts of the theoretically expected and the experimentally reconstructed tomographs of the $\langle\psi_1| = (0, 0, 0, 0, 1, 0, 0, 0)$ state in the eight-dimensional quantum system, with an experimental state fidelity of 0.97.

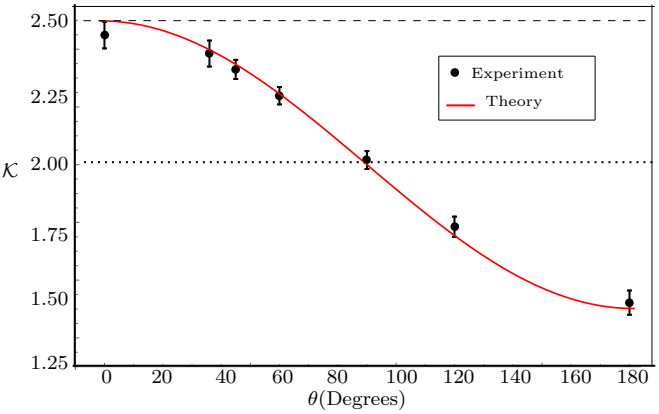

FIG. 10. Graph representing quantum correlations corresponding to the inequality $\mathcal{K}$ for various states rotated by the angle θ from the initial state $|\psi\rangle$.

TABLE VI. Theoretically computed and experimentally measured values of quantum correlations corresponding to the inequality $\mathcal{K}$ for various states, rotated by the angle θ, from the initial state $|\psi\rangle$.

θ	Theory	Expt.
180°	1.500	1.522 ± 0.042
120°	1.750	1.785 ± 0.035
90°	2.000	2.016 ± 0.031
60°	2.250	2.239 ± 0.030
45°	2.353	2.330 ± 0.033
36°	2.404	2.385 ± 0.045
0°	2.500	2.449 ± 0.046

π refocusing pulses. The durations of the $\frac{\pi}{2}$ pulses for ^{1}H, ^{19}F, and ^{13}C nuclei were 9.36 μs at a power level of 18.14 W, 23.25 μs at a power level of 42.27 W, and 15.81 μs at a power level of 179.47 W, respectively.

The quantum circuit to construct the states required to test fully contextual quantum correlations is shown in Fig. 8(a) and the corresponding NMR pulse sequence is shown in Fig. 8(b). Different states can be prepared by varying the value of the flip angle θ of the rf pulse. We prepared seven different states by varying the flip angle θ to attain a range of values: 180°, 120°, 90°, 60°, 45°, 36°, and 0°. The state prepared with $\theta = 180°$ gives the minimum value of $\mathcal{K}$, while the state prepared without applying any rf pulse ($\theta = 0°$) gives the maximum value. All the states required to demonstrate the KCBS twin inequality on an eight-dimensional Hilbert space which are capable of revealing the transformation from classical correlations to fully contextual correlations were experimentally prepared with state fidelities greater than or equal to 0.96. The tomograph of one such experimentally reconstructed state with flip angle $\theta = 180°$ with state fidelity 0.97 is depicted in Fig. 9. For each of the initial states, the contextuality test was repeated three times. The mean values and the corresponding error bars were computed and the results are shown in Fig. 10, where the inequality values are plotted for different values of the parameter θ. The maximum of the sum of probabilities using classical theory is 2 and the maximum of the sum of probabilities using quantum theory is 2.5; they are depicted by dotted and dashed lines, respectively, in Fig. 10. The theoretically computed and experimentally obtained values of the inequality for different values of the θ parameter are tabulated in Table VI. The theoretical and experimental values match well, within the limits of experimental errors. From Fig. 10 it can also be seen that the violation observed for the KCBS twin inequality decreases as the original state $|\psi\rangle$ is rotated through an angle θ, with no violation when the transformed state is orthogonal to the original state. Furthermore, the plot is nonlinear, indicating that smaller rotations lead to minor changes in violation, while larger rotations may also lead to observing no violation at all.

IV. CONCLUSION

In this paper we experimentally demonstrated fully contextual quantum correlations on an NMR quantum information processor. We studied two distinct inequalities capable of revealing such correlations: The first inequality used ten measurements on a four-dimensional Hilbert space while the second inequality used five measurements on an eight-dimensional Hilbert space to reveal fully contextual correlations. However, both inequalities involved the same number of projectors. For an experimental demonstration of each inequality, every projector was decomposed in terms of the Pauli basis and the corresponding inequality recast in terms of Pauli operators, thereby reducing the need for resource-intensive full state tomography. Both inequalities $\mathcal{C}$ and $\mathcal{K}$ were experimentally implemented with a fidelity greater than or equal to 0.96 by measuring the expectation values of only five and seven Pauli operators, respectively, for the state which maximizes the violation.

In addition to demonstration of fully contextual quantum correlations, we analyzed the behavior of each inequality under rotation of the underlying state, which unitarily transforms it to another pure state. The experiments were repeated for various states rotated through an angle θ and were in good agreement with theoretical results. It was seen that both the inequalities follow a nonlinear trend, while the inequality $\mathcal{K}$ offers a greater range of violation than the inequality $\mathcal{C}$ with respect to the parameter θ.

An experimental implementation of fully contextual quantum correlations is an important step towards achieving information processing tasks, for which no postquantum theory can do better. While the inequality $\mathcal{C}$ has been experimentally observed in optical systems, an experimental demonstration of the inequality $\mathcal{K}$ is difficult owing to the high dimensionality of the Hilbert space required. Our work asserts that NMR is an optimal test bed for such scenarios.

ACKNOWLEDGMENTS

J.S. acknowledges funding from University Grants Commission, India. Arvind acknowledges funding from Department of Science and Technology, New Delhi, India under Grant No. EMR/2014/000297. K.D. acknowledges funding from Department of Science and Technology, New Delhi, India under Grant No. EMR/2015/000556.

APPENDIX A: DECOMPOSITION OF THE PROJECTORS APPEARING IN THE INEQUALITY $\mathcal{C}$

The decomposition of the projectors Π_i appearing in the inequality $\mathcal{C}$ in terms of two-qubit Pauli operators is given as

$$\Pi_0 = \tfrac{1}{4}(-ZI - ZX + IX + II), \tag{A1a}$$
$$\Pi_1 = \tfrac{1}{4}(XI - XX - IX + II), \tag{A1b}$$
$$\Pi_2 = \tfrac{1}{4}(-XI + XX - IX + II), \tag{A1c}$$
$$\Pi_3 = \tfrac{1}{4}(-XX + YY + ZZ + II), \tag{A1d}$$
$$\Pi_4 = \tfrac{1}{4}(XI + XX + IX + II), \tag{A1e}$$
$$\Pi_5 = \tfrac{1}{4}(-XI + XZ - IZ + II), \tag{A1f}$$
$$\Pi_6 = \tfrac{1}{4}(-XZ + YY - ZX + II), \tag{A1g}$$
$$\Pi_7 = \tfrac{1}{4}(XX - YY + ZZ + II), \tag{A1h}$$
$$\Pi_8 = \tfrac{1}{4}(XZ + YY + ZX + II), \tag{A1i}$$
$$\Pi_9 = \tfrac{1}{4}(-XZ - YY + ZX + II), \tag{A1j}$$

TABLE VII. Pauli operators for three qubits used to decompose the corresponding projectors for the experimental demonstration of the inequality $\mathcal{K}$.

Pauli operators	Pauli operators
$A_0 = IIX$	$A_{17} = XZX$
$A_1 = IIZ$	$A_{18} = XZZ$
$A_2 = IXI$	$A_{19} = YIY$
$A_3 = IXX$	$A_{20} = YXY$
$A_4 = IXZ$	$A_{21} = YYI$
$A_5 = IYY$	$A_{22} = YYX$
$A_6 = IZI$	$A_{23} = YYZ$
$A_7 = IZX$	$A_{24} = YZY$
$A_8 = IZZ$	$A_{25} = ZII$
$A_9 = XII$	$A_{26} = ZIX$
$A_{10} = XIX$	$A_{27} = ZIZ$
$A_{11} = XIZ$	$A_{28} = ZXI$
$A_{12} = XXI$	$A_{29} = ZXX$
$A_{13} = XXX$	$A_{30} = ZXZ$
$A_{14} = XXZ$	$A_{31} = ZYY$
$A_{15} = XYY$	$A_{32} = ZZI$
$A_{16} = XZI$	$A_{33} = ZZX$
$A_{34} = ZZZ$	$A_{35} = III$

where I, X, Y, and Z are identity operators and σ_x, σ_y and σ_z Pauli operators.

APPENDIX B: DECOMPOSITION OF PROJECTORS APPEARING IN INEQUALITY $\mathcal{K}$

The decomposition of the projectors Π_i appearing in the inequality $\mathcal{K}$ in terms of three-qubit Pauli operators is given as

$$\Pi_0 = \tfrac{1}{16}[-A_0 + A_1 + 2A_6 - A_7 + A_8 + \sqrt{2}(A_9 - A_{10} + A_{11} + A_{16} - A_{17} + A_{18} - A_{19} - A_{24}) - A_{26} - A_{27} - A_{33} - A_{34} + 2A_{35}], \tag{B1a}$$

$$\Pi_1 = \tfrac{1}{32}[-\sqrt{3}A_0 - A_1 + 2A_3 - 2A_5 + 2A_6 - \sqrt{3}A_7 + A_8 + \sqrt{2}(-A_9 + \sqrt{6}A_{10} - A_{11} + \sqrt{6}A_{12} - A_{13} - \sqrt{6}A_{14} + A_{15} - A_{16} + \sqrt{6}A_{17}) + \sqrt{2}(-A_{18} - \sqrt{6}A_{19} - A_{20} + \sqrt{6}A_{21} - A_{22} - \sqrt{6}A_{23} - \sqrt{6}A_{24}) + \sqrt{3}A_{26} + A_{27} + 2A_{29} - 2A_{31} - 2A_{32} + \sqrt{3}A_{33} + 3A_{34} + 4A_{35}], \tag{B1b}$$

$$\Pi_2 = \tfrac{1}{8}(-A_4 + A_5 - A_7 + A_{25} - A_{30} + A_{31} - A_{33} + A_{35}), \tag{B1c}$$

$$\Pi_3 = \tfrac{1}{8}(A_4 - A_5 - A_7 + A_{25} + A_{30} - A_{31} - A_{33} + A_{35}), \tag{B1d}$$

$$\Pi_4 = \tfrac{1}{32}[-\sqrt{3}A_0 - A_1 - 2A_3 + 2A_5 + 2A_6 - \sqrt{3}A_7 + A_8 + \sqrt{2}(-A_9 + \sqrt{6}A_{10} - A_{11} - \sqrt{6}A_{12} + A_{13} + \sqrt{6}A_{14} - A_{15} - A_{16} + \sqrt{6}A_{17}) + \sqrt{2}(-A_{18} - \sqrt{6}A_{19} + A_{20} - \sqrt{6}A_{21} + A_{22} + \sqrt{6}A_{23} - \sqrt{6}A_{24}) + \sqrt{3}A_{26} + A_{27} - 2A_{29} + 2A_{31} - 2A_{32} + \sqrt{3}A_{33} + 3A_{34} + 4A_{35}], \tag{B1e}$$

$$\Pi_5 = \tfrac{1}{32}[\sqrt{3}A_0 + A_1 - 2A_2 - 2A_4 + 2A_6 + \sqrt{3}A_7 - A_8 + \sqrt{2}(-A_9 - \sqrt{6}A_{10} - A_{11} + A_{12} + \sqrt{6}A_{13} + A_{14} + \sqrt{6}A_{15} - A_{16} - \sqrt{6}A_{17}) + \sqrt{2}(-A_{18} + \sqrt{6}A_{19} - \sqrt{6}A_{20} + A_{21} + \sqrt{6}A_{22} + A_{23} + \sqrt{6}A_{24}) - \sqrt{3}A_{26} + 3A_{27} - 2A_{28} - 2A_{30} - 2A_{32} - \sqrt{3}A_{33} + A_{34} + 4A_{35}], \tag{B1f}$$

$$\Pi_6 = \tfrac{1}{32}[\sqrt{3}A_0 + A_1 + 2A_2 + 2A_4 + 2A_6 + \sqrt{3}A_7 - A_8 + \sqrt{2}(-A_9 - \sqrt{6}A_{10} - A_{11} - A_{12} - \sqrt{6}A_{13} - A_{14} - \sqrt{6}A_{15} - A_{16} - \sqrt{6}A_{17}) + \sqrt{2}(-A_{18} + \sqrt{6}A_{19} + \sqrt{6}A_{20} - A_{21} - \sqrt{6}A_{22} - A_{23} + \sqrt{6}A_{24}) - \sqrt{3}A_{26} + 3A_{27} + 2A_{28} + 2A_{30} - 2A_{32} - \sqrt{3}A_{33} + A_{34} + 4A_{35}], \tag{B1g}$$

$$\Pi_7 = \tfrac{1}{8}(A_4 + A_5 + A_7 + A_{25} + A_{30} + A_{31} + A_{33} + A_{35}), \tag{B1h}$$

$$\Pi_8 = \tfrac{1}{16}[A_0 + A_1 + 2A_6 + A_7 + A_8 + \sqrt{2}(A_9 + A_{10} + A_{11} + A_{16} + A_{17} + A_{18} + A_{19} + A_{24}) + A_{26} - A_{27} + A_{33} - A_{34} + 2A_{35}], \tag{B1i}$$

$$\Pi_9 = \tfrac{1}{8}(-A_4 - A_5 + A_7 + A_{25} - A_{30} - A_{31} + A_{33} + A_{35}), \tag{B1j}$$

where the A_i's are given in Table VII.

[1] J. S. Bell, Rev. Mod. Phys. **38**, 447 (1966).
[2] S. Kochen and E. P. Specker, J. Math. Mech. **17**, 59 (1967).
[3] J. Singh, K. Bharti, and Arvind, Phys. Rev. A **95**, 062333 (2017).
[4] R. Raussendorf, Phys. Rev. A **88**, 022322 (2013).
[5] M. Howard, J. Wallman, V. Veitch, and J. Emerson, Nature (London) **510**, 351 (2014).
[6] A. Cabello, Nature (London) **474**, 456 (2011).
[7] A. Cabello, Phys. Rev. A **87**, 010104(R) (2013).
[8] G. Chiribella, G. M. D'Ariano, and P. Perinotti, Phys. Rev. A **84**, 012311 (2011).
[9] H. Barnum, S. Beigi, S. Boixo, M. B. Elliott, and S. Wehner, Phys. Rev. Lett. **104**, 140401 (2010).
[10] M. Pawlowski, T. Paterek, D. Kaszlikowski, V. Scarani, A. Winter, and M. Zukowski, Nature (London) **461**, 1101 (2009).
[11] A. Peres, J. Phys. A: Math. Gen. **24**, L175 (1991).

[12] A. R. Plastino and A. Cabello, Phys. Rev. A **82**, 022114 (2010).
[13] P. Badziąg, I. Bengtsson, A. Cabello, and I. Pitowsky, Phys. Rev. Lett. **103**, 050401 (2009).
[14] A. Cabello, M. Kleinmann, and C. Budroni, Phys. Rev. Lett. **114**, 250402 (2015).
[15] A. A. Klyachko, M. A. Can, S. Binicioğlu, and A. S. Shumovsky, Phys. Rev. Lett. **101**, 020403 (2008).
[16] P. Kurzyński and D. Kaszlikowski, Phys. Rev. A **86**, 042125 (2012).
[17] A. Sohbi, I. Zaquine, E. Diamanti, and D. Markham, Phys. Rev. A **94**, 032114 (2016).
[18] C. Zu, Y.-X. Wang, D.-L. Deng, X.-Y. Chang, K. Liu, P.-Y. Hou, H.-X. Yang, and L.-M. Duan, Phys. Rev. Lett. **109**, 150401 (2012).
[19] V. D'Ambrosio, I. Herbauts, E. Amselem, E. Nagali, M. Bourennane, F. Sciarrino, and A. Cabello, Phys. Rev. X **3**, 011012 (2013).
[20] E. Amselem, M. Rådmark, M. Bourennane, and A. Cabello, Phys. Rev. Lett. **103**, 160405 (2009).
[21] E. Nagali, V. D'Ambrosio, F. Sciarrino, and A. Cabello, Phys. Rev. Lett. **108**, 090501 (2012).
[22] Y.-F. Huang, M. Li, D.-Y. Cao, C. Zhang, Y.-S. Zhang, B.-H. Liu, C.-F. Li, and G.-C. Guo, Phys. Rev. A **87**, 052133 (2013).
[23] X. Zhang, M. Um, J. Zhang, S. An, Y. Wang, D.-l. Deng, C. Shen, L.-M. Duan, and K. Kim, Phys. Rev. Lett. **110**, 070401 (2013).
[24] F. M. Leupold, M. Malinowski, C. Zhang, V. Negnevitsky, A. Cabello, J. Alonso, and J. P. Home, Phys. Rev. Lett. **120**, 180401 (2018).
[25] H. Bartosik, J. Klepp, C. Schmitzer, S. Sponar, A. Cabello, H. Rauch, and Y. Hasegawa, Phys. Rev. Lett. **103**, 040403 (2009).
[26] O. Moussa, C. A. Ryan, D. G. Cory, and R. Laflamme, Phys. Rev. Lett. **104**, 160501 (2010).
[27] S. Dogra, K. Dorai, and Arvind, Phys. Lett. A **380**, 1941 (2016).
[28] E. Amselem, L. E. Danielsen, A. J. López-Tarrida, J. R. Portillo, M. Bourennane, and A. Cabello, Phys. Rev. Lett. **108**, 200405 (2012).
[29] A. Singh, H. Singh, K. Dorai, and Arvind, Phys. Rev. A **98**, 032301 (2018).
[30] A. Gaikwad, D. Rehal, A. Singh, Arvind, and K. Dorai, Phys. Rev. A **97**, 022311 (2018).
[31] I. S. Oliveira, T. J. Bonagamba, R. S. Sarthour, J. C. C. Freitas, and E. R. deAzevedo, *NMR Quantum Information Processing* (Elsevier, Oxford, 2007).
[32] H. Singh, Arvind, and K. Dorai, Phys. Rev. A **95**, 052337 (2017).
[33] A. Mitra, K. Sivapriya, and A. Kumar, J. Magn. Reson. **187**, 306 (2007).
[34] J. Zhang, A. M. Souza, F. D. Brandao, and D. Suter, Phys. Rev. Lett. **112**, 050502 (2014).
[35] G. M. Leskowitz and L. J. Mueller, Phys. Rev. A **69**, 052302 (2004).
[36] H. Singh, Arvind, and K. Dorai, Phys. Lett. A **380**, 3051 (2016).